Nanofabrication via Atom Optics

C.C. Bradley, W.R. Anderson, J.J. McClelland, and R.J. Celotta
Electron Physics Group, National Institute of Standards and Technology,

Gaithersburg, MD 20899

Send Proofs to:

J.J. McClelland

Electron Physics Group, National Institute of Standards and Technology

Gaithersburg, MD 20899

Ph: 301-975-3721

Fax: 301-926-2746

Email: jabez.mcclelland@nist.gov

Nanofabrication via Atom Optics

C.C. Bradley, W.R. Anderson, J.J. McClelland, and R.J. Celotta

Abstract

Owing to the continuing reduction in the scale of microelectronic and micromagnetic technology, new microfabrication methods are constantly being explored. This is particularly true in the case of nanostructure fabrication. Here, the phenomenon of optical diffraction limits the resolution obtainable by exposing a photoresist to a pattern of light, as is done in conventional lithography. We are investigating a different paradigm. Since both light and matter can be thought of as waves, instead of focusing light waves with objects made of matter, why not focus matter waves with objects made of light? To accomplish this we use lasers to form lenses from optical waves. These lenses focus a beam of neutral atoms prior to the atom's deposition on a silicon substrate. In this way, we have fabricated chromium structures consisting of thousands of parallel lines or millions of dots with dimensions as small as 28 nanometers. We describe the basis of this new technology, present examples of its application to date, detail its advantages and limitations, and discuss the future of optical nanostructure fabrication.

Continued demand for the miniaturization of electronic, magnetic and mechanical components will require the invention of new techniques for fabrication of sub-micron devices. Atom-optical manipulation of neutral atoms has recently been explored as a possible means for building structures on the nanoscale. Using light to focus atoms as they are deposited on surfaces is a striking reversal of conventional lithographic methods, where atoms (in lenses and masks) are used to focus light onto resist-coated substrates. There are several reasons for focusing matter waves instead of light waves to build nanostructures. Since atoms from thermal sources have small (~pm) de Broglie wavelengths, the diffraction-limited resolution for atom focusing can be on the nanoscale. Also, growing structures from focused atom beams can be regarded as an intrinsically direct-write lithographic process, eliminating resists and other chemical processing that result in contamination. Further, with deposition of focused atom beams, precise parallel patterning of large areas with nanostructures is readily attainable with the atomic manipulation methods developed to date.

A particular atom-optical scheme that has been investigated in some detail utilizes the light force exerted on atoms as they travel through a near-resonant standing wave laser field. Using laser beams that graze the substrate surface, several experiments have shown that deposited atoms can be concentrated into features smaller than 100 nm. This was first demonstrated using sodium[i], and subsequently with chromium in one[ii,iii] and two[iv,v] dimensions, and also with aluminum[vi].

We discuss here recent work on laser-focused deposition using chromium atoms. The essential geometry of these experiments is shown in Fig. 1. A laser beam is directed across the surface of a substrate and retroreflected to make a standing wave. Crossing

perpendicular to the standing wave, a highly collimated beam of atoms is incident on the surface. The laser wavelength λ is chosen to correspond to a strong resonance in the atom: λ = 424.55 nm (vacuum wavelength) for Cr, corresponding to the $^7S \leftrightarrow {}^7P$ transition. As the laser is tuned near resonance, the light induces an electric dipole moment in the atom. This dipole is acted upon by the laser field to produce a force that is proportional to, and directed along, the gradient of the light intensity[vii]. With a positive detuning, in our case 500 MHz, atoms are pushed toward the nodes of the field. Near each node the force is approximately proportional to the atom's displacement from the field zero, due to the nearly quadratic spatial dependence of the standing wave intensity in these regions. Consequently, a laser standing wave should act like a series of lenses, with each lens separated by the node spacing of $\lambda/2$[viii].

To obtain the smallest possible deposited features, the atomic beam is collimated before it enters the standing wave by application of transverse laser cooling, as shown in Fig. 2. Using the same mirror that retroreflects the standing wave (thereby ensuring alignment), a laser beam detuned below the atomic resonance by one natural linewidth (5 MHz for Cr) is reflected with orthogonal polarization (the *lin $\perp$ lin* configuration) to create a polarization-gradient cooling region[ix]. This provides a collimation sufficient for 90% of all atoms in the beam to be contained in an angular spread of 0.6 mrad[x].

As illustrated in Fig. 2, chromium atoms effuse from a commercial high-temperature source held near 1850 K. The atom beam formed by a 1 mm diameter nozzle and a downstream 1mm-square aperture, is laser-collimated and then deposited through the 500 MHz-detuned standing wave. The standing wave detuning is provided by the frequency shift of an acousto-optic modulator (AOM). After deposition of a laser-

focused Cr pattern on a substrate (typically Si, but also sapphire and GaAs have been used), the sample is removed from vacuum and examined with an atomic force microscope (AFM) in air. Figure 3 shows what is seen in the region of the sample covered by the laser beam: a regular array of lines with 212.78 nm period and highly uniform height and width. The height of the lines is primarily a function of the atomic beam intensity and the deposition time. The width of the lines is a sensitive function of the atomic beam collimation and the standing wave intensity, profile and detuning. As shown in Fig. 3, these parameters were adjusted to obtain a full-width-at-half-maximum (FWHM) of 38 nm. In subsequent studies, we have produced lines as narrow as 28 nm FWHM[xi].

The parallel fabrication of such precise arrays of nanometer-scale lines may be useful for such diverse applications as nanoscale length standards, optical grating fabrication, or perhaps in the development of novel sensors. Of course, to improve the usefulness of laser-focused atomic deposition, techniques for making more complex patterns are needed. While creation of completely arbitrary structures is still in the future, we have been able to create two-dimensional arrays of dots[xii], and also reduce the line spacing from $\lambda/2$ to $\lambda/8$[xiii].

The two-dimensional square array of dots is formed by superimposing two standing waves intersecting at 90° above the substrate. To simplify the experiment, interference between the two standing waves is prevented by use of orthogonal polarizations in the crossed beams. An AFM image of the resulting two-dimensional pattern is shown in Fig. 4. The dot spacing is $\lambda/2 = 212.78$ nm. For the example shown, the peak-to-valley height is 13 nm and the dot full-width is 80 nm. If the resolution can

be significantly improved, a simple and useful extension would be to translate the sample within the λ/2 unit cell of the array during deposition, resulting in the parallel fabrication of large arrays of arbitrary patterns. This capability would greatly enhance the versatility of the process.

Reduced-period arrays can also be fabricated, as shown in Figure 5. This example, with a line spacing of λ/8 (or 53 nm) was produced by taking advantage of a subtle effect in the laser-atom interaction[xiii]. Instead of using a simple, linearly-polarized standing wave, the polarization of the reflected laser beam is rotated 90° by inserting a quarter-wave plate in front of the retroreflection mirror. This creates a *lin ⊥ lin* standing wave, which can be regarded as two circularly-polarized standing wave components (σ+ and σ-) with nodes offset by λ/4. The resulting laser-atom interaction is described by two arrays of potential wells with periodicity λ/2, offset by λ/4. Focusing of atoms occurs not only in all these wells, creating a λ/4 periodicity, but also in the crossings of the wells at odd multiples of λ/8. The crossings focus atoms because they are actually avoided crossings by coherent coupling induced by Raman transitions between the seven magnetic sub-levels of the Cr ground state.

While laser-focused deposition can produce nanostructures that are useful objects or artifacts themselves, the technique may be combined with other processing steps to build a much wider range of interesting structures. As a demonstration of one such possible use, we have used laser-focused chromium lines to fabricate an array of magnetic nanowires[xiv]. Nanoscale patterning of magnetic materials is of great current interest not only for technological reasons, pertaining to magnetic recording media, but also scientific reasons, stemming from interest in the behavior of magnetic particles with

very small dimensions and high aspect ratios. By evaporating iron at a grazing angle of 10°, sufficient shadowing was caused by the Cr peaks to result in an array of distinct Fe wires with width approximately 40 nm, height approximately 5 nm, spacing 212.78 nm, and length up to 150 μm.

To observe the magnetic ordering of this array of iron wires, we examined it with scanning electron microscopy with polarization analysis (SEMPA)[xv]. This technique allows the magnetization of a surface to be examined with the lateral resolution of a scanning electron microscope. Figure 6 contains an image taken over a 10 μm × 10 μm region, clearly showing the iron lines with domains of magnetization either "up" (white), or "down" (black). The gray regions between the white or black lines correspond to the non-magnetic chromium underlayer, which is visible between the iron depositions. The very large length-to-width ratio of the magnetic wires results in a strong uniaxial shape anisotropy, which forces the magnetization to point along the wires. Thus we have, in essence, an array of one-dimensional magnets that can be studied in greater detail.

As a demonstration of another possible extension, we have explored the modification of laser-focused structures by reactive-ion etching (RIE)[xvi]. RIE is a powerful tool for patterning semiconductor materials such as silicon or GaAs. Highly anisotropic etching can be achieved with a suitable choice of resist and plasma conditions, creating deep structures with smooth, straight sidewalls. Chromium is known to be an excellent resist material for RIE. A complication is that the deposited patterns sit on top of a uniform Cr background, typically ranging from one-half to one-fourth the height of the peaks. This background results from imperfections in the atom focusing and from other isotopes in the atom beam that do not interact with the laser (16% of the

atoms). Despite the fact that this material reduces the pattern contrast and so interferes with the preferential etching of the substrate, we find regular patterns etched into the silicon substrate. Figure 7 shows several scanning electron microscope (SEM) images of a sample etched for 17 minutes in a 50 W RF plasma with a 7.5×10^{-6} mol/sec (10 sccm) flow of SF_6 and a base pressure of 2.3 Pa (17 mtorr). With a single sample we can study the effect of the reduced contrast via the differences in chromium deposition across the Gaussian profile of the standing wave laser beam. The image in Fig. 7a shows the highest contrast region of the sample. Here, the chromium is reduced to an array of very narrow (nominally 68 nm wide) wires on top of etched Si peaks. The figure shows that some of the wires have broken free. Not shown are nearby large areas where the wires remain intact. Figure 7b shows the result of intermediate Cr contrast. In this region we find relatively flat Cr "ribbons" nominally 100 nm wide, separated by trenches in the silicon nominally 200 nm deep as determined from cross-section SEM images[xvi]. Figure 7c shows the result for low contrast. Here, the sputtering just broke through the background thickness in the valleys, so the pattern consists of a Cr film cut by a uniform array of narrow trenches nominally 40 nm wide and 90 nm deep.

As mentioned earlier, the utility of laser-focused deposition would be greatly enhanced with improved resolution and the consequent reduction of the minimum feature size. To investigate the resolution limit of this process we have explored the roles played by experimental parameters, such as the input laser beam intensity and alignment, and have observed subtle effects due to the details of Cr film growth.

To examine the role played by laser intensity, and hence potential depth, in focusing atoms, we have made a series of measurements as a function of laser intensity.

As discussed above, differences in the deposition due to variation of the intensity across the laser beam are recorded in a single deposition sample. Making use of the input laser's Gaussian profile, a series of AFM images at different substrate positions is obtained and correlated to the input laser intensity at each location, denoted by $I_{TW}(x,0)$. Feature widths are obtained by averaging AFM linescans over 1μm-square regions of the sample. In Fig. 8a, we show the intensity dependence of the feature width[xvii] for the case where half of the incident laser beam is blocked by the substrate (schematically depicted by the figure inset). As the intensity increases from zero, Fig. 8a shows a decrease in the feature width up to an intensity of about 2 W/mm^2[xviii], above which there is a gradual broadening. The feature width minimum occurs at the intensity that brings the atom lens into focus for the most probable velocity in the atom beam. The data shown in Fig. 8b were taken in the same manner as the data in Fig. 8a, except that the standing wave was shifted away from the substrate by one $1/e^2$ beam radius (60 μm). Numerical modelling of the atomic flux at the surface is shown by the dotted curves in the figure. For both data sets in Fig. 8, there is excellent agreement between the shape of the experimental data and the numerical calculation. The depositions used for Fig. 8 were of 5 minutes duration to produce an average Cr thickness of 4 nm.

The most likely explanation for the offset between the calculations and the experiment shown in Fig. 8, lies in the behavior of the chromium on the surface during and after deposition. To study this further we looked at the dependence of the feature width on the amount of Cr deposited, which we controlled by varying the duration of deposition. If the atoms are stationary after landing on the substrate, we expect the

feature width to be independent of the average chromium thickness. Instead, we find a marked dependence on total amount of chromium deposited.

In Fig. 9, the measured feature width is plotted as a function of average chromium thickness with the various symbols representing data taken in separate but nominally equivalent runs. We see that as a function of thickness, the width has a value near 55 nm at very low thickness, then decreases, going through a minimum near 3 nm average thickness. After the minimum, the width rises steadily to a value of about 70 nm at 24 nm average thickness. The absolute minimum FWHM observed is 28 ±1 nm for an average Cr thickness of 3±0.4 nm thickness. The variation in line width is quite surprising, considering the near refractory nature of chromium and the fact that the depositions were conducted at room temperature. A possible explanation for the decreasing feature width at low coverage is that a higher mobility of Cr on the substrate material is slowly being replaced by a lower mobility of Cr on the Cr surface. The increase in width from the minimum can perhaps be attributed to an increase in chromium grain size with chromium thickness, once a significant amount of Cr is built up on the surface. Such an increase in grain size with chromium film thickness has been observed in other studies[xix].

To further clarify the role of growth, we also examined the behavior of the width of features on samples where a uniform layer of chromium was applied directly over corrugated Cr nanostructured films. Experimentally, we simply applied a uniform layer immediately after the laser-focused deposition. The goal was to simplify the deposition, in order to clearly demonstrate the redistribution of the atoms and the consequent change in shape of the Cr features.

To perform this experiment, two laser-focused depositions were modified by depositing a uniform layer of chromium (overlayer) on top of the patterned depositions (base-layer). The two patterned base layers were deposited for different durations, yielding different initial profiles. One deposition contained features that were 30 nm wide with 4 nm peak-to-valley height. The features on the other deposition were nominally 65 nm wide by 35 nm high. The sample was then translated to a new position so that half of the base-layer for each deposition was exposed to the atom flux from the oven. The standing wave laser was blocked while a uniform layer of chromium (~20 nm) was deposited. Due to the geometry of a physical aperture and the atom beam divergence, the overlayer thickness varies from 0 to 20 nm over a transition region ~150 microns long. After the deposition, we took a series of AFM images by stepping through the transition region, in order to measure the feature width dependence on overlayer thickness.

The data is presented in Fig. 10 as the broadening (increase in the FWHM) of the features versus overlayer thickness. Both samples, each with different base-layer features but identical over-layers are shown in the figure differentiated by plot symbol. For each sample, we see an increase in the broadening from 0 to 10 nm as chromium is added to the overlayer, up to a thickness of 20 nm. The broadening is the same in each case even though the initial feature shapes were quite different. This provides additional evidence that Cr growth plays an important role in the observed broadening of laser-focused chromium depositions. Such growth might be explained by invoking processes involving grain formation, governed by differing rates for diffusion up vs. down an atomic step edge[xx].

We have demonstrated that it is possible to fabricate sub-30 nm (FWHM) features with chromium. It is apparent that further reduction of the minimum feature size will require detailed investigation of growth phenomena using well-characterized substrate surfaces and controlled deposition conditions. With improved control over the growth conditions or surface chemistry, we may hope to realize the full potential of laser-focused deposition. In that case, improvement in resolution would result from using a source of mono-energetic atoms instead of a thermal atom beam. To that end, we have laser-cooled and trapped chromium atoms in a magneto-optic trap (MOT)[xxi]. In this first realization of a Cr MOT, atoms were evaporated from a resistively-heated, Cr-plated, tungsten filament, located about 2 cm from the MOT center. Judging from trap fluorescence, we estimate that over 10^4 atoms are routinely collected in the MOT from the nearby filament source. Recent work has been to supply atoms to the Cr MOT from a laser-slowed atom beam and to investigate optical pumping of Cr atoms between the states involved in laser-cooling and trapping and untrapped metastable states.

We have described advances made in the generalization of the laser-focused atomic deposition techniques to include increasingly complex patterns and also fabrication in other materials besides chromium. These demonstrations indicate the potential of this technique, and also that there is much research to be done regarding atom-optical phenomena, surface growth and diffusion, and materials issues. Atom optics is a relatively new field and there is still much to learn regarding the interaction of atoms with complex light fields. With the creation of bright monochromatic sources of atoms it will be possible to determine the ultimate resolution limits of atom focusing and to manipulate atoms in other ways (such as atom holography[xxii]). Finally, a detailed

understanding of surface growth and diffusion is critical to these efforts since no matter how small a focal spot is obtained atom-optically, atom behavior on surfaces will ultimately determine the shape and size of fabricated structures. New research in these and other areas is the key to tapping the potential of atom optics for nanofabrication.

Figure Captions

FIG. 1. Focusing of atoms in the nodes of a laser standing wave for deposition of nanoscale features on a substrate.

FIG. 2. Schematic of the experimental layout used in laser-focused atom deposition.

FIG. 3. Atomic force microscope (AFM) images of chromium line nanostructures formed by laser-focused atom deposition. (a) 1 μm-square image of a relatively thin deposition onto a silicon substrate, showing lines with an average full-width of 38 nm. (b) 8 μm-square image of a thicker deposition on sapphire, illustrating the long-range uniformity of the lines.

FIG. 4. Atomic force microscope (AFM) image of a two-dimensional array of chromium "dots" produced by laser-focused deposition using crossed orthogonal standing waves.

FIG. 5. Atomic force microscope (AFM) image of chromium lines with $\lambda/8$ spacing produced by focusing atoms in a *lin $\perp$ lin* standing wave. The average pitch is 53.2 nm.

FIG. 6. Magnetic nanowires formed by evaporation of iron at grazing incidence onto chromium line nanostructures. The image is taken with scanning electron

microscopy with polarization analysis (SEMPA), which is sensitive to the surface magnetization. In this image, black and white indicate opposite magnetization directions along the lines. The gray regions reveal the non-magnetized chromium substrate between the iron wires.

FIG. 7. Scanning electron microscope (SEM) images showing reactive-ion etched chromium/silicon nanostructures. (a) Region of relatively small background and large peak-to-valley height (strong contrast) in the original deposition produced narrow (68 nm diameter) wires on top of sharp silicon ridges; (b) region of intermediate original contrast produced well-separated Cr ribbons; (c) region of low original Cr contrast produced narrow trenches cut into the silicon (the brightest features are the trench walls).

FIG. 8. Feature width as a function of laser intensity for the case when (a) the center of the incident Gaussian laser profile intercepts the substrate surface and (b) when the center of the incident Gaussian laser beam is separated from the substrate surface by one beam waist (60 μm). Each case is graphically represented by the inset diagrams. The dotted lines are the result of a numerical ray-tracing model evaluated at several intensities. The width uncertainties are typically $\pm$2-3 nm, about the size of the plotted symbols for the data.

FIG. 9. Feature width as a function of Cr thickness. To determine the average Cr thickness the samples are masked and etched and then re-imaged with the AFM. Symbols differentiate data taken on separate runs.   Uncertainty in the measured average Cr thickness results from the etching procedure and is the same for all the data points. Uncertainty in the measured feature width results from image statistics and AFM tip effects (the latter worsening with height for sharp surface features).

FIG. 10. Feature width as a function of Cr overlayer thickness. The square symbols give the broadening that was observed for a base-layer consisting of chromium lines measuring 30 nm FWHM by 4 nm peak-to-valley height. The circles give the broadening for a base-layer with lines measuring 65 nm wide by 35 nm high. The diagrams above the plots are example AFM linescans of the base-layer and overlayer for each case, the shaded region showing the overlayer material. Uncertainty in the feature broadening is estimated as ±5-10% of the measured widths.

Figures
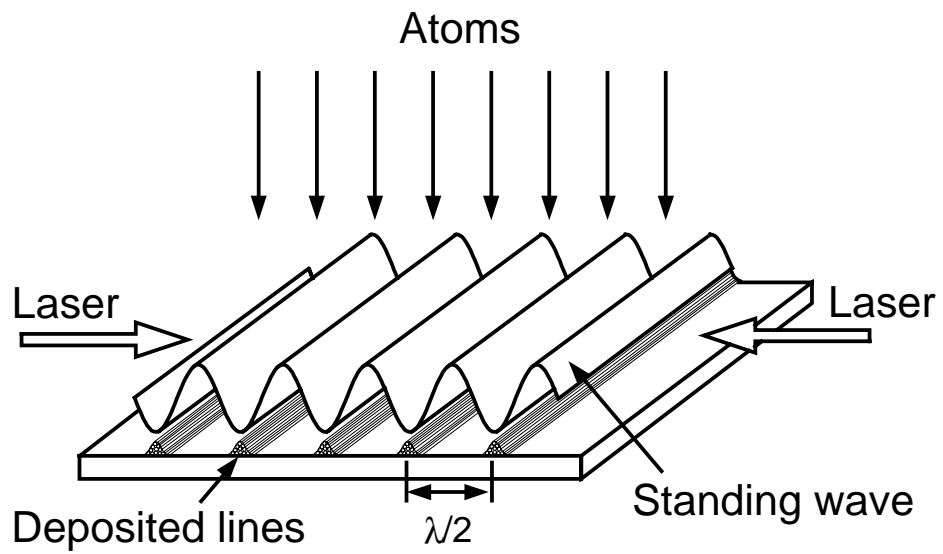
Figure 1.

Figure 2.

Figure 3.
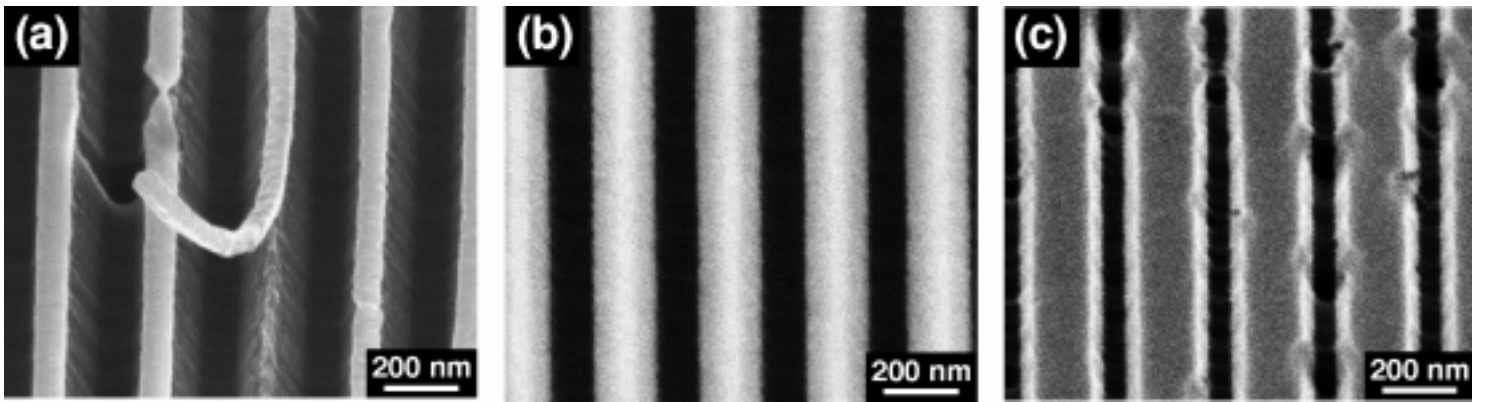
212.78 nm

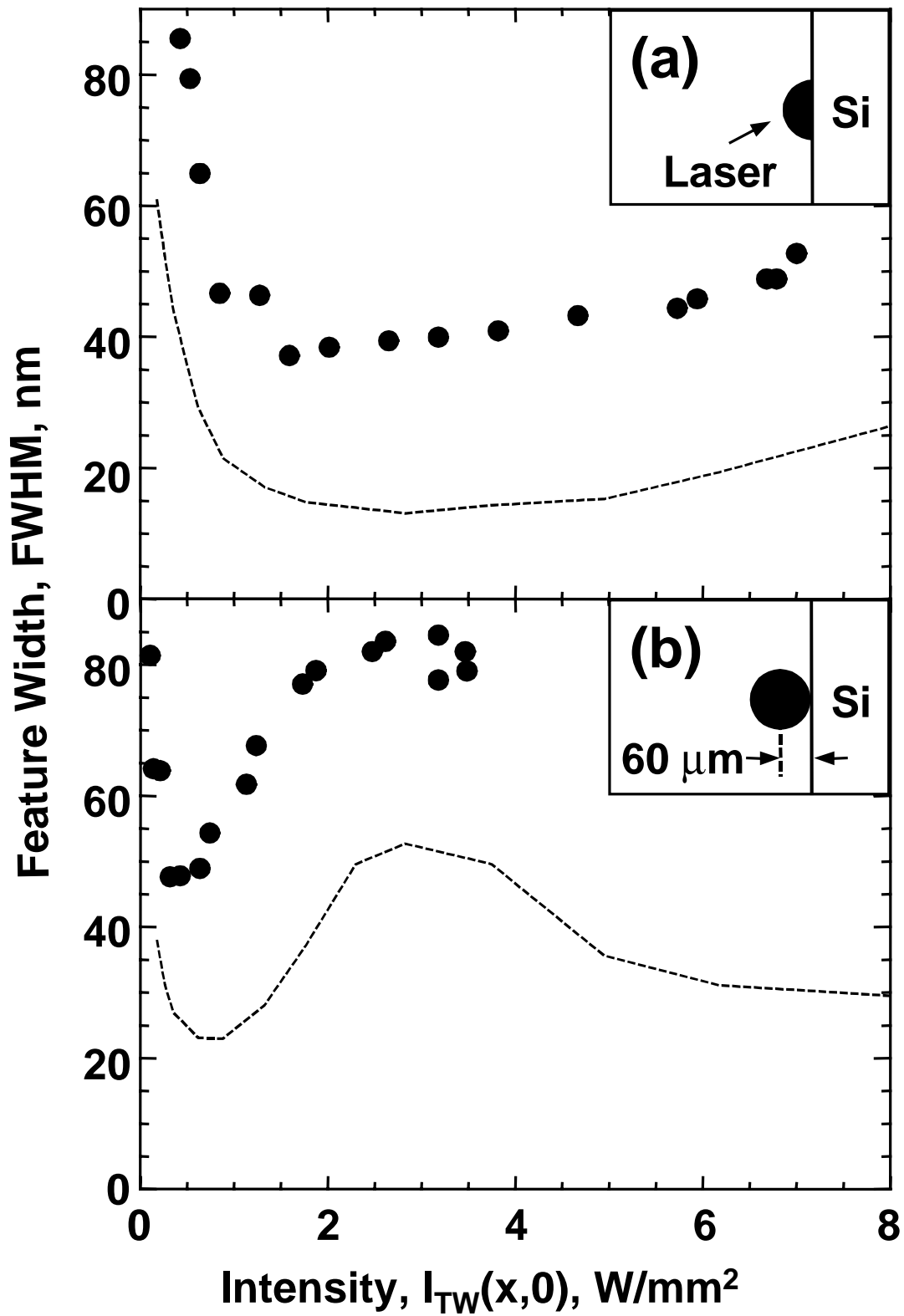13 nm

Figure 4.
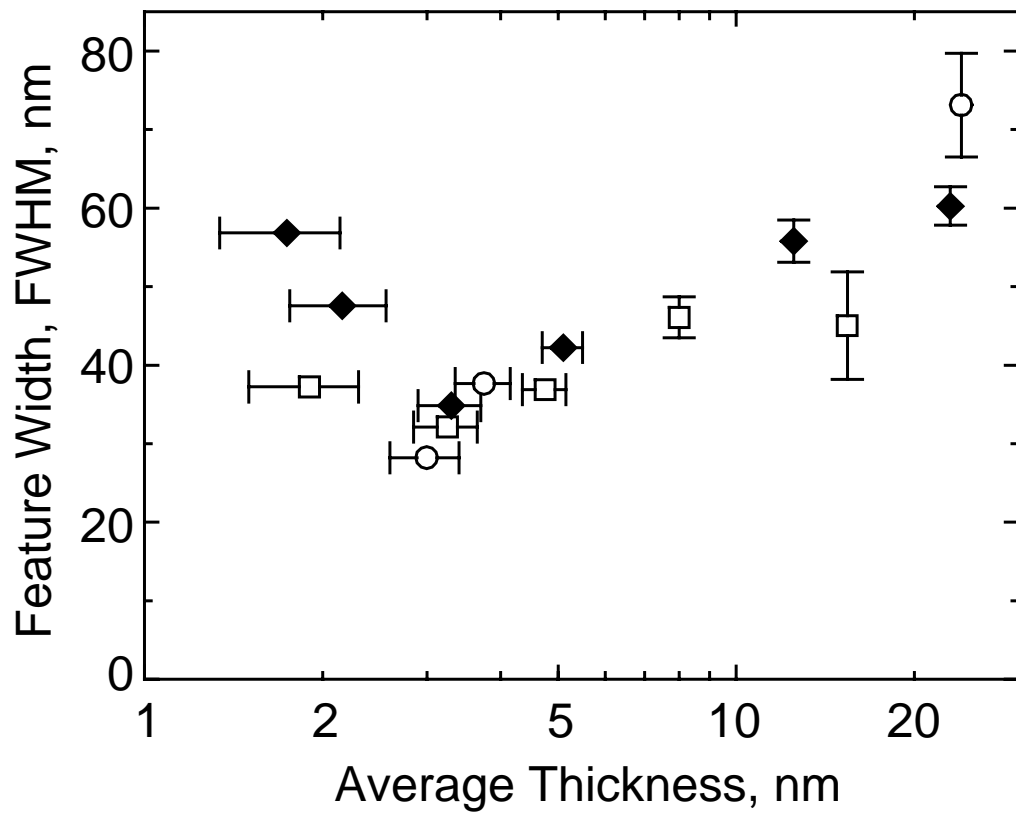
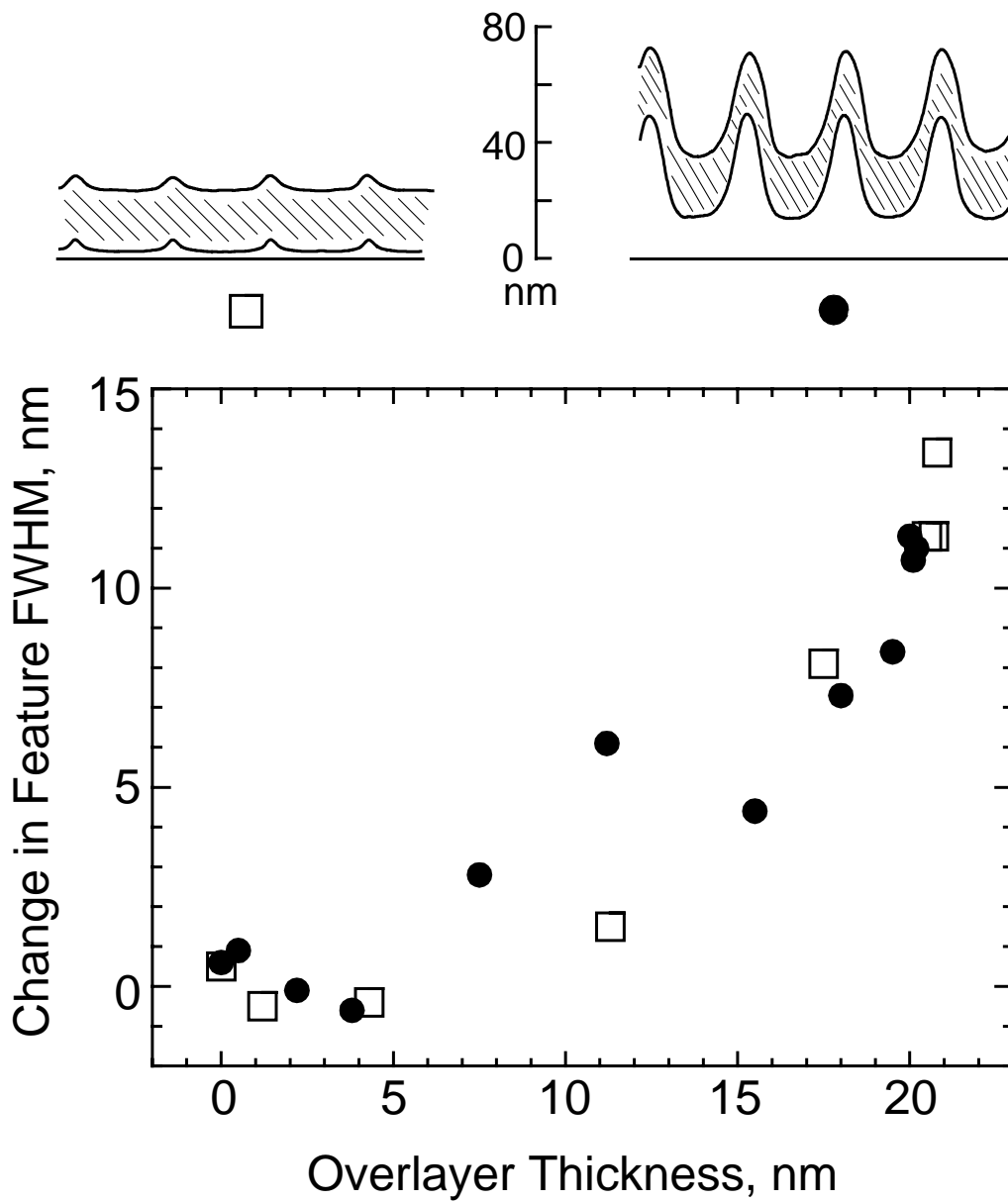**200 nm**
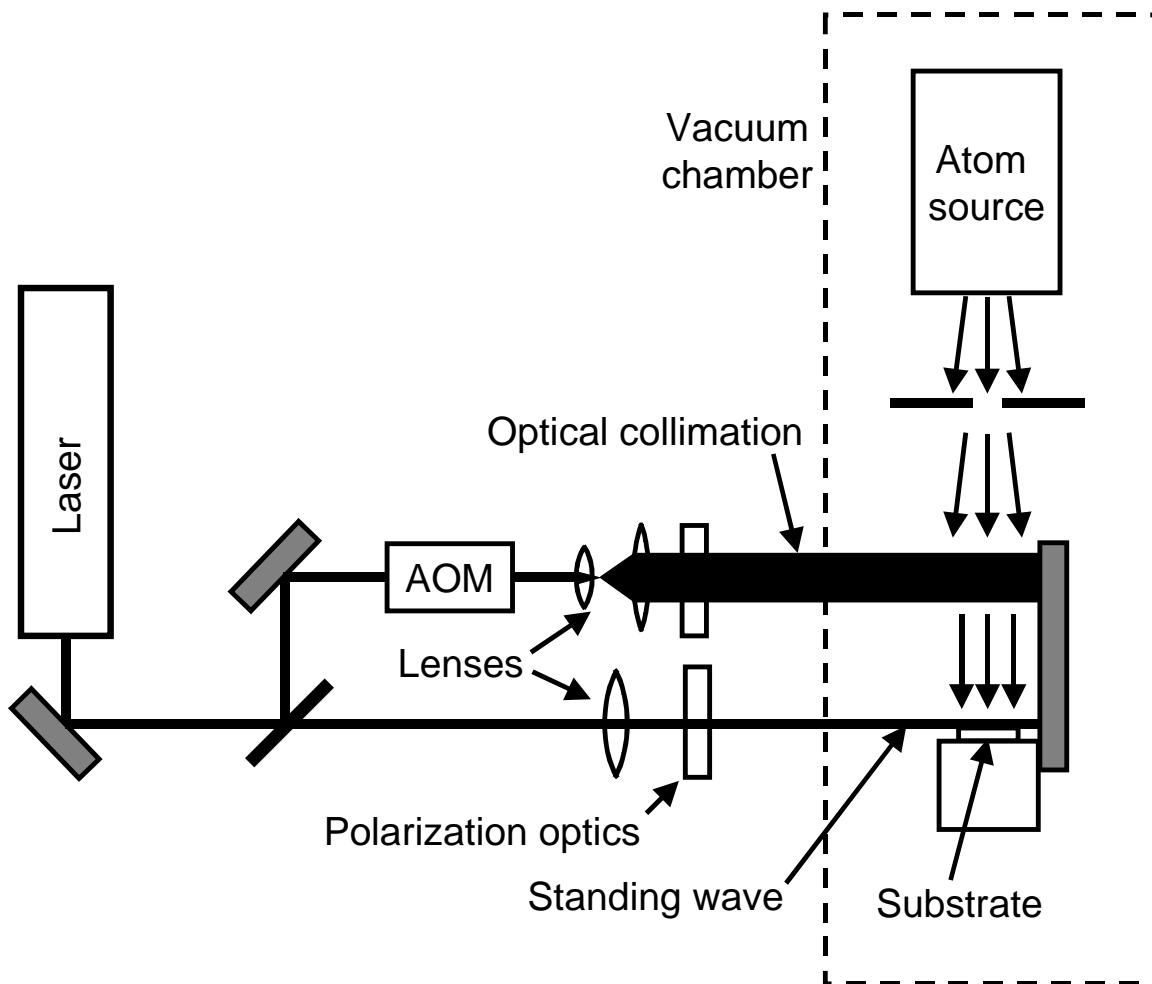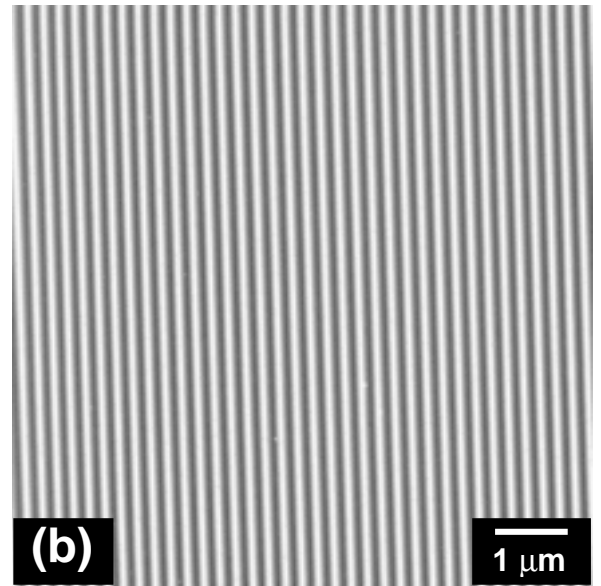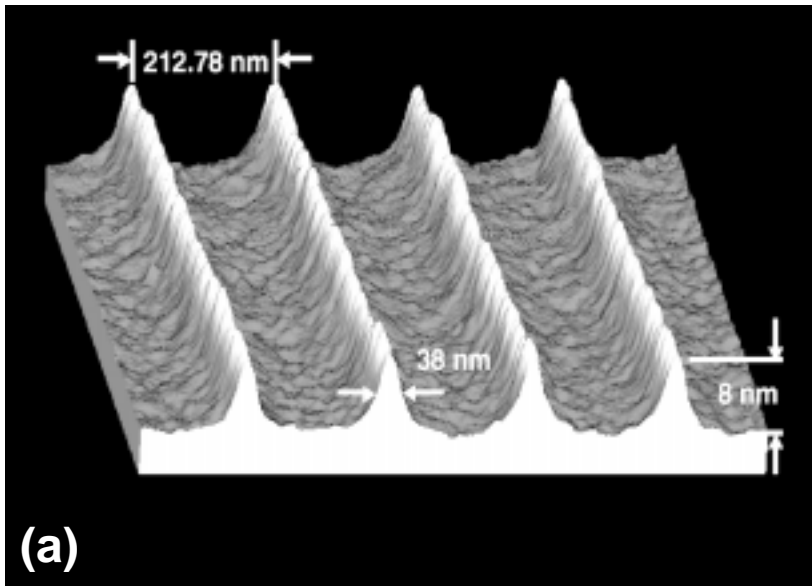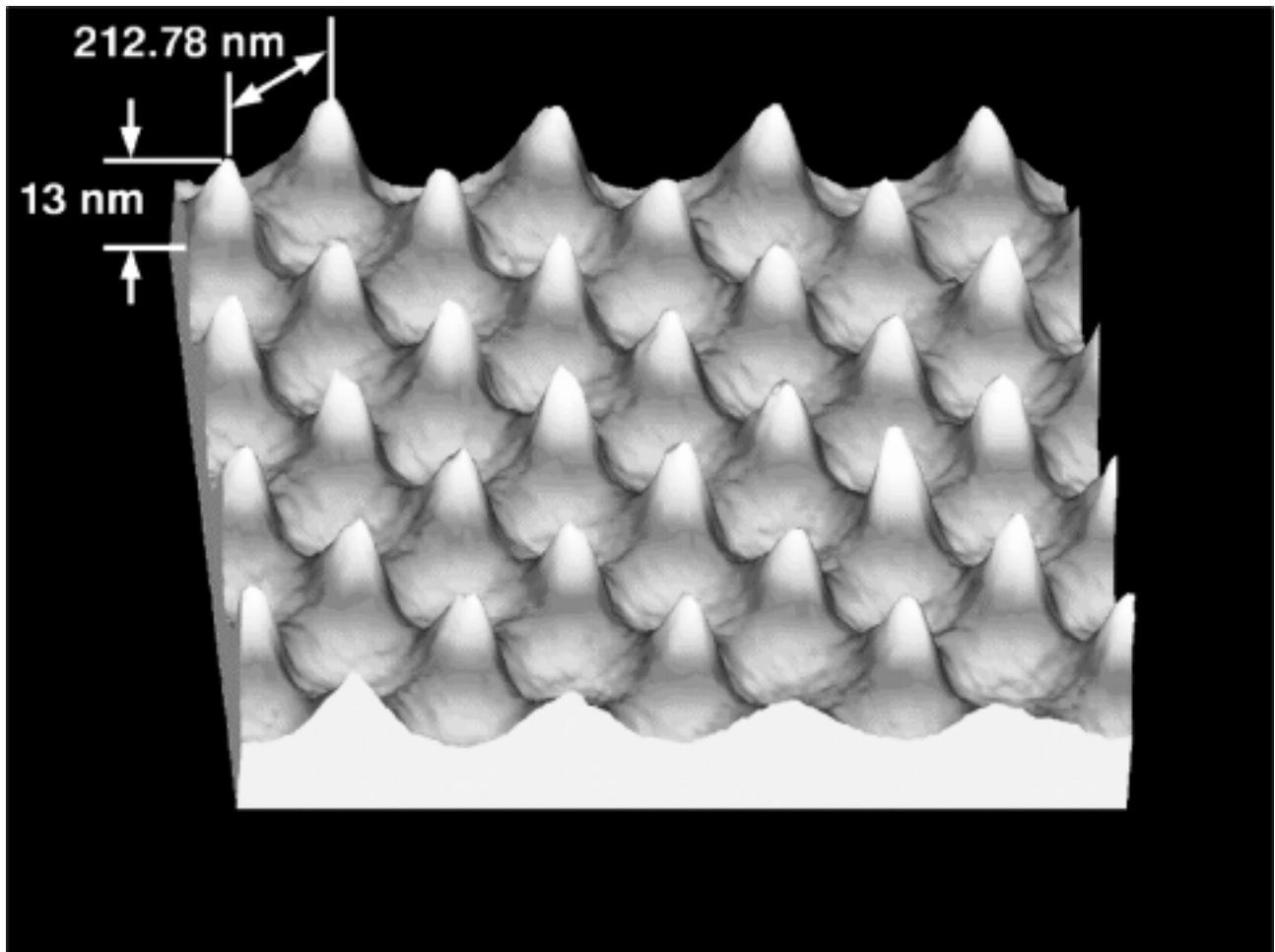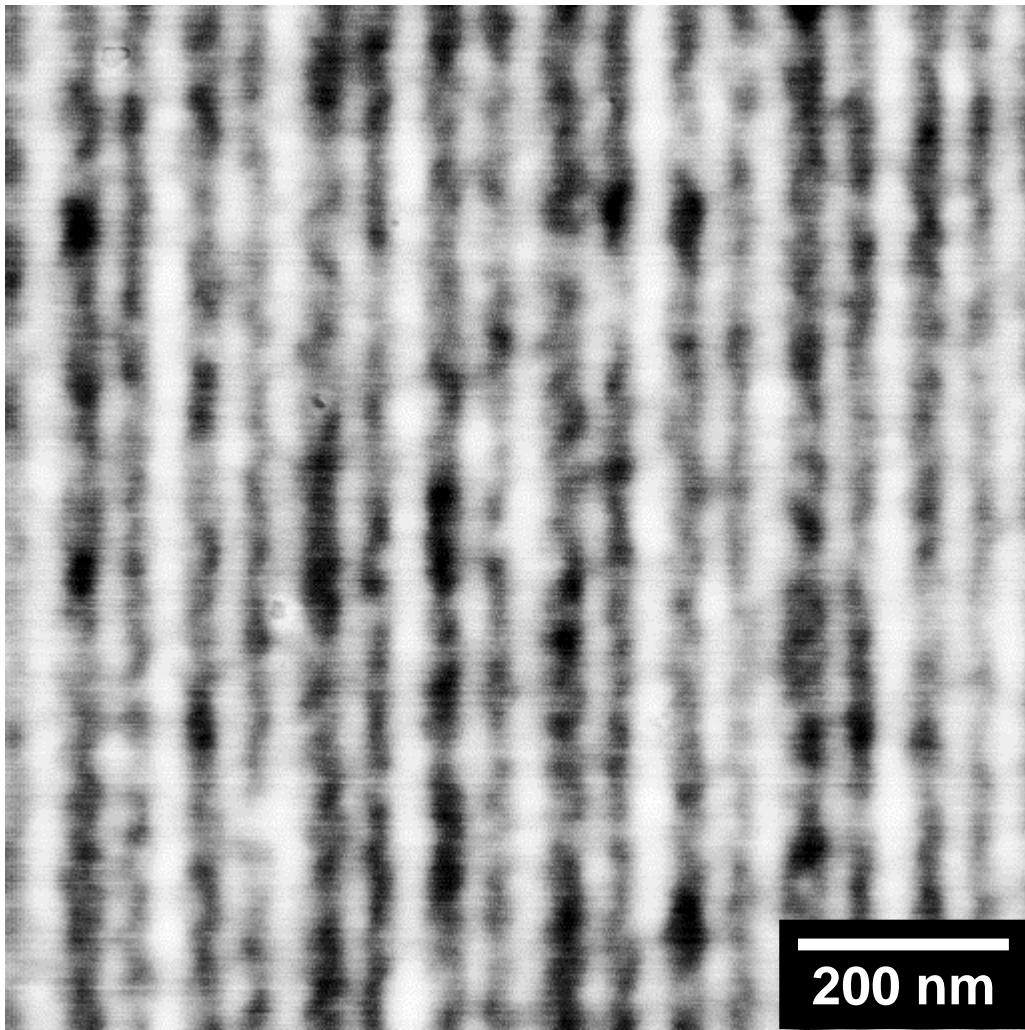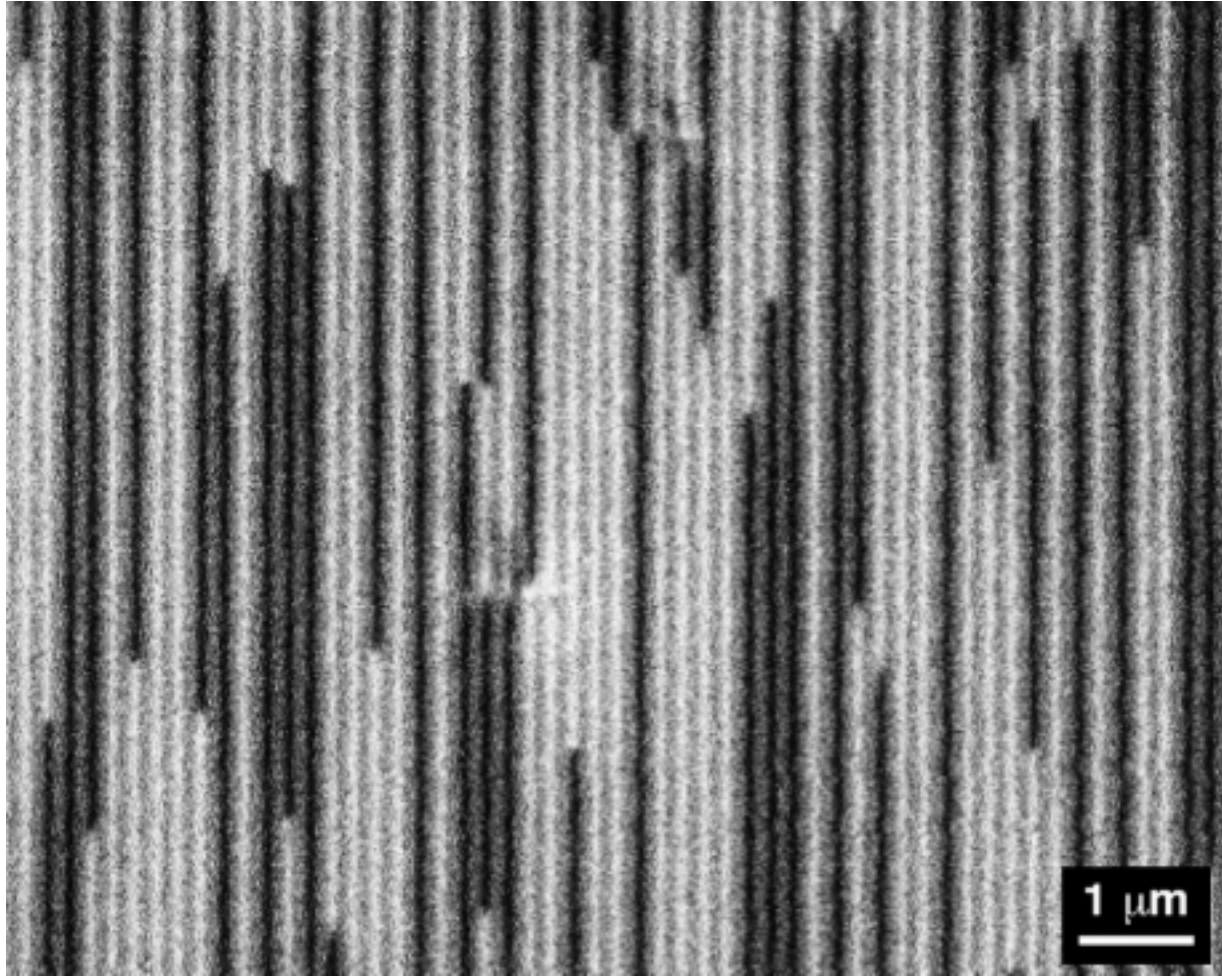
Figure 5.

Figure 6.

Figure 7.

Figure 8.

Figure 9.

Figure 10.

[i] G. Timp, R.E. Behringer, D.M. Tennant, J.E. Cunningham, M. Prentiss, and K.K. Berggren, Phys. Rev. Lett. **69**, 1636 (1992).

[ii] J.J. McClelland, R.E. Scholten, E.C. Palm, and R.J. Celotta, Science **262**, 877 (1993).

[iii] U. Drodosfsky, J. Stuhler, B. Brezger, Th. Schulze, M. Drewsen, T. Pfau, and J. Mlynek, Microelectron. Eng. **35**, 285 (1997).

[iv] R. Gupta, J.J. McClelland, Z.J. Jabbour, and R.J. Celotta, Appl. Phys. Lett. **67**, 1378 (1995).

[v] U. Drodofsky, J. Stuhler, Th. Schulze, M. Drewsen, B. Brezger, T. Pfay, and J. Mlynek, Appl. Phys. B **65**, 755 (1997).

[vi] R.W. McGowan, D.M. Giltner, and Siu Au Lee, Opt. Lett. **20**, 2535 (1995).

[vii] J. P. Gordon and A. Ashkin, Phys. Rev. A **21**, 1606 (1980).

[viii] J. J. McClelland, J. Opt. Soc. Am. B **12**, 1763 (1995).

[ix] J. Dalibard and C. Cohen-Tannoudji, J. Opt. Soc. Am. B **6**, 2023 (1989).

[x] R. E. Scholten, R. Gupta, J. J. McClelland, R. J. Celotta, M. S. Levenson, and M. G. Vangel, Phys. Rev. A **55,** 1331 (1997).

[xi] W.R. Anderson, C.C. Bradley, J.J. McClelland, and R.J. Celotta (manuscript in preparation).

[xii] R. Gupta, J. J. McClelland, Z. J. Jabbour, and R. J. Celotta, Appl. Phys. Lett. **67**, 1378 (1995).

[xiii] R. Gupta, J. J. McClelland, P. Marte, and R. J. Celotta, Phys. Rev. Lett. **76**, 4689 (1996).

[xiv] D.A. Tulchinsky, M.H. Kelley, J.J. McClelland, R. Gupta, and R.J. Celotta, J. Vac. Sci. Technol. A, **16**, 1817 (1998).

[xv] M. R. Scheinfein, J. Unguris, M. H. Kelley, D. T. Pierce, and R. J. Celotta, Rev. Sci. Instrum. **61**, 2501 (1990).

[xvi] J. J. McClelland, R. Gupta, R. J. Celotta, and G. A. Porkolab, Appl. Phys. B **66**, 95 (1998).

[xvii] In the data presented there is an uncertainty in the quoted widths of ±5-10% due to statistical variation of the deposited lines over the area imaged by the AFM.

[xviii] The intensity values presented have an uncertainty of about 10%, primarily due to laser power measurement uncertainty.

[xix] D. Goyal, A.H. King, and J.C. Bilello, Mat. Res. Symp. Proc., **108**, 395 (1988).

[xx] J. Villain, J. Phys. I (France) **1**, 19 (1991); I. Elkinani and J. Villain, J. Phys. I (France) **4**, 949 (1994).

[xxi] C.C. Bradley, W.R. Anderson, J.J. McClelland, and R.J. Celotta, Bull. Am. Phys. Soc. **43**, 1291 (1998).

[xxii] J. Fujitsa, M. Morinaga, T. Kishimoto, M. Yasuda, S. Matsui, and F. Shimizu, Nature **380**, 691 (1996).